Article

Surface Tension Estimation of Steel above Boiling Temperature

Joerg Volpp [1,2]

1   Department of Engineering Sciences and Mathematics, Luleå University of Technology, 971 87 Luleå, Sweden;
     jorg.volpp@hv.se
2   Department of Engineering Science, University West, 461 86 Trollhattan, Sweden

Abstract: Surface tension is an important characteristic of materials. In particular at high temperatures, surface tension values are often unknown. However, for metals, these values are highly relevant in order to enable efficient industrial processing or simulation of material behavior. Plasma, electron or laser beam processes can induce such high energy inputs, which increase the metal temperatures to, and even above, boiling temperatures, e.g., during deep penetration welding or remote cutting. Unfortunately, both theoretical and experimental methods experience challenges in deriving surface tension values at high temperatures. Material models of metals have limitations in explaining complex ion interactions, and experimentally measuring temperature and surface tension at high temperatures is a challenge for methods and equipment. Therefore, surface wave analysis was conducted in this work to derive surface tension values around the boiling temperature of steel and identify trends. In addition, a simple ion interaction calculation was used to simulate the impacting parameters that define the surface tension. Since both the experimental values and simulation results indicate an increasing trend in surface tension above the boiling temperature, it is concluded that the dominating attractive forces above this temperature should increase with increasing temperature and lead to increasing surface tension forces in the surface layers of liquid metal.

Keywords: liquid metal; laser beam; vaporization; surface tension estimation; surface wave measurement; ion interaction

1. Introduction

Surface tension is a material property that defines many material behaviors during, e.g., wetting phenomena or induction of the Marangoni effect. Many high temperature material processing techniques (e.g., brazing, welding, cutting, Additive Manufacturing) also include surface tension effects. During brazing, the wetting behavior and the resulting shape of the track are defined by surface tension in combination with other surface properties and thermal aspects [1]. In welding, surface appearance is influenced by surface tension and can even lead to undercuts [2]. In addition, the root weld seam is defined by surface tension effects, which can lead to instabilities [3] and underfill [4]. During laser deep penetration, the typical vapor channel appears, in which surface tension forces from the surrounding boiling metal surface counteract the recoil pressure from the laser-induced ablation [5]. In the new metal Additive Manufacturing processes, surface tension defines the track appearances and the material incorporation through the melt surfaces [6]. However, often the surface tension values are not available at such high temperatures and are extrapolated or estimated. These estimations are necessary, e.g., during material simulations [7], but denote a source of uncertainty on the results. In addition, quality predictions can be difficult when the input parameters are unknown or imprecise. A more precise description or measurement of surface tension values is, therefore, highly demanded.

Surface tension can be described as a force within the surface layer parallel to a liquid surface. The main sources are the attractive forces between atoms or molecules in the surface layer [8]. Surface tension is described by two models: (1) the energy necessary to integrate molecules or atoms from the bulk material into its surface in order to enlarge it

(energy per area, unit: J/m^2) [9]; (2) the resistance to a force when lengthening a liquid surface (force per length, unit N/m).

However, a surface cannot be understood as a sharp transition, but consists of several atomic distances [10]. Lennard-Jones and Dent [11] concluded that surfaces should contract to enable the necessary density reduction closer to the surface. In addition, it was shown that surface layering can occur for some metals, which can be seen as a transition zone with atomic distance variations of a few atomic layers [12–14]. These surface layer oscillations are related to the metallic character of the binding interactions and many-body effects [15,16]. Based on these theories, material models for metals were developed describing the surface layer of liquid metals as ions embedded into a background electron gas [17], based on the Fermi–Dirac statistics. The surface tension can be derived as the negative pressure of the electron gas. Unfortunately, describing metal interactions is not easy, and simple Lennard-Jones potentials alone cannot usually be applied to describe and model the short-range non-additive electron exchange interactions of ion metal bonding [18,19]. Therefore, liquid metals must be modelled as ions embedded in an electron jellium with the support of quantum mechanical considerations (e.g., [20,21]).

It is known that the surface tension decreases at increasing temperature for most pure materials [22]. Surface tension data are often only available at or just above melting temperature. Liquid iron measurements were recorded up to ~2500 K [23]. Often, a linear decrease in surface tension values is assumed at increasing temperature based on measurements around melting temperatures and assumed linear behavior (e.g., [22]). For example, measured surface tension values of iron σ_{Fe} in a highly pure Argon atmosphere [24] give a temperature T dependent linear equation

$$\sigma_{Fe} = (1925 \pm 65)\frac{N}{m} - (0.455 \pm 0.034)\frac{N}{m \cdot K} \cdot (T - 1808K) \tag{1}$$

The partly observed surface tension decrease is related to the increasing vibration of the atoms and molecules and the increasing distance between them, leading to reduced attractive forces. More complex situations arise when alloying elements are present, which can even lead to a change in slope of the surface tension (e.g., [25]). At even higher temperatures further above the melting temperature, only very little data are available from experimental measurements and theoretical predictions are difficult. The main reason is that the impact of phenomena and interactions, at and above boiling temperature, on surface tension have not yet been sufficiently described. Effects, such as vaporization of atoms or ionic bonds are, however, known to be non-linear effects [26]. Therefore, a simple linear extrapolation of data points from temperatures where those effects play a minor role is not very likely to be sufficient. In addition, it seems unlikely that a linear decrease is possible, since that would indicate that the surface tension decreases to and below zero at some point.

In general, at increasing temperatures, thermal expansion happens, which increases the atomic distances. The increasing distance between the ions should lead to a lower surface tension, as the literature assumes. However, thermal expansion appears due to the asymmetric curvature of the potential energy trough [27] and the Fermi band broadening might induce counteracting force [28,29], since the ions show a higher probability of having more conduction electrons at increasing temperature. This effect can increase the ion charge and, thereby, the Coulomb forces [30]. In total, these effects can lead to an increased surface tension. The additional effect of extensive vaporization on boiling surfaces, where atoms are ejected from the surface [31], is scarcely explored but can be expected to create 'holes' in the surface layer. The effect of such a lack of atoms in surface on surface tension is still unclear but can probably affect the surface tension, due to missing bonding forces.

Surface tension measurements are necessary to evaluate and validate models. There are several surface tension measurement methods categorized as: (1) direct measurement using microbalance, (2) measurement of capillary pressure, (3) capillary-gravity force analysis, (4) gravity-distorted drops and (5) reinforced drop distortion [32]. The measurement of

liquid metals is limited to, e.g., the maximum bubble pressure method, measuring the pressure peak while a gas bubble inside the liquid material is formed. Another possibility is the observation of liquid droplets (e.g., the sessile drop method [33]) wetting a surface of another material. However, this method contains potential measurement errors related to the interfacial tension, which is often not known, and surface roughness.

Due to the practical measuring challenges at high temperatures, non-contact methods are often preferred for measuring surface tension of liquid metals. Levitated drops [34,35] or falling drops can be used. The frequency of the oscillations of falling drops can give surface tension values (e.g., [36]). Measuring the surface tension at even higher temperatures than recorded up to ~2500 K (e.g., [25,37,38]) is challenging. Another method to derive surface tension values is the relation of surface wave propagation characteristics on liquid metals to surface tension [39]. These methods are contactless and are, therefore, in general also suitable to be used at high temperatures. Usable surface waves for such methods must propagate based on restoration by surface tension. This is given at Bond numbers Bo $\ll$ 1. In this regime, the Kelvin relation [40] can be used to derive the surface tension. For the relation to surface tension, the wave frequency, wavelength, and material density need to be measured or known [41]. Fortunately, the Kelvin equation can be used for a wide temperature range [42]. The impact of several sources of uncertainty were evaluated, e.g., the vapor recoil pressure was shown to have neither a stabilizing nor destabilizing effect on the melt pool surface waves and does not impact the measurement [43]. The Marangoni flow can slightly decrease the surface wave frequencies [44].

However, it can be difficult to create environments at high temperatures that enable identification of relevant features for surface tension measurements. It is a challenge to create a calm and homogeneous material surface at temperatures around the boiling point of metals without inducing additional effects that can disturb the measurements, such as evaporation of the surface [27].

Besides experimental methods, surface tension can be simulated using atom interaction calculations or molecular dynamic simulations. However, these calculations can also show high uncertainties and fluctuations due to the complexity of the induced physical processes and interactions [45]. In general, detailed molecular dynamic simulations require high calculation times, e.g., embedded atom calculations require many steps, since the embedded atom changes its embedding energy and the interaction distances to all other atoms ([45]). Often, ~10^6 atoms are used for simulations (e.g., [46]). Pressure and density results are typically evaluated after several hundred picoseconds of simulation time and averaged over ~100 ps [47] to derive values with <0.1% deviation [46]. The number of calculation steps can exceed 20,000, while simulation results often lie 20–40% below the measured values [45] or, for cohesive work calculations, even 30–40% above [48]. Calculations of aluminum systems showed a decreasing trend in surface tension at increasing temperature, but show higher values compared to other authors' measurements and simulations [49]. A possible reason for such deviations can be the large electron-density gradients at the surface [47]. Even though understanding of and approaches to simulations have increased, current models still experience issues describing metal surface tension and in connecting macroscopic effects to particle interactions [50].

Therefore, this work aims to derive high-temperature (above boiling temperature) surface tension values using an indirect experimental measurement method and a comparison to a simple physical material surface model to reveal trends in surface tension effects at such high temperatures. A laser-induced melt pool is suggested for the experimental surface tension derivation, which enables a certain control of the surface temperature, using the laser power and illumination time, which other methods cannot provide. New high-speed imaging possibilities at very high frame rates enable the recording of surface waves, which can then be related to local surface tension values. In combination with temperature estimations, trends in surface tension at increasing temperatures are suggested.

2. Materials and Methods

Surface tension values were determined using experimental surface wave analysis of laser-induced melt pools (similar to in previous experiments [51]), and simplified ion interaction calculations.

2.1. Surface Wave Analysis

A stationary laser beam from a fibre laser (IPG YLR-15000, IPG Photonics, Burbach, Germany, wavelength 1070 nm) was aimed towards a steel plate (Docol 200, SSAB, Stockholm, Sweden), illuminated by a laser pulse of 1 s duration with 1.5 kW laser output power at a defocussed spot size of ~2.1 mm (Figure 1). Argon shielding gas at a flow rate of ~10 L/min was used. The metal surface was observed using a high-speed camera (Photron Fastcam Mini UX100 type 800K-M-16G, Reutlingen, Germany) at 10,000 fps with a bandpass filter that only transmits the reflections from the processing zone of the used illumination laser (Cavitar, continuous wave, 808 nm wavelength, multimode, no preferred polarization, spot diameter on the material of ~10 mm).
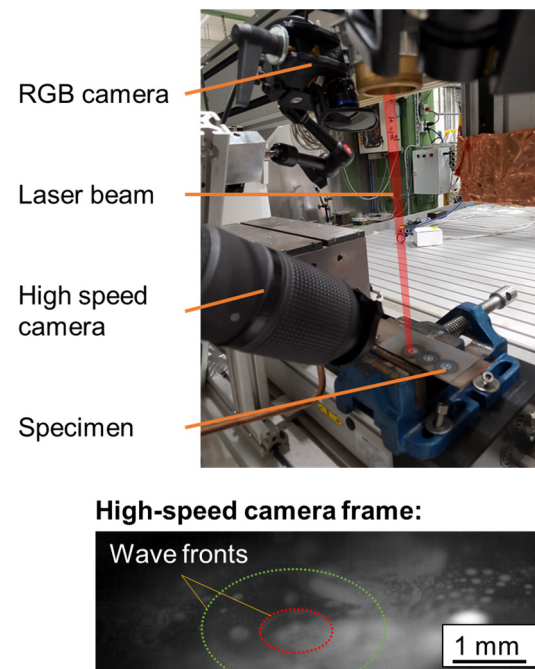

Figure 1. Set-up to create a controlled melt pool using laser beam heating, observed by an RGB camera for temperature calculations and a high-speed camera to observe melt pool surface wave propagations.

When a surface event occurred on the surface, e.g., initiated by a degassing gas bubble, the resulting surface waves were observed and evaluated. Their frequencies f and wavelengths λ were determined from the video frames (Figure 1). The assumptions were that small values of disturbance occur, the surface tension is constant over the oscillating surface, and the liquid is uniform in depth, incompressible and irrotational at small wave amplitudes. These assumptions enable the use of the Kelvin equation [40]. Due to the small wavelengths of the capillary waves compared to the liquid film depth, reliable surface tension data σ_k can be derived by [40]

$$\sigma_k = \frac{\rho}{k^3} \cdot \left(4\pi^2 \cdot f^2 - g \cdot k \right) \qquad (2)$$

while f is the frequency related to the angular frequency $\omega = 2\pi \cdot f$ and $k = \frac{2\pi}{\lambda}$ the wave vector. The error in measuring the frequencies and wavelengths λ leads to uncertainties in the surface tension measurements. Type B uncertainties were estimated. Deviation Δ

was assumed to be symmetrical. Uncertainties u_B were derived for each surface tension measurement according to

$$u_B = \frac{\Delta}{\sqrt{3}} \tag{3}$$

The relative uncertainties $\widetilde{u}_B$ were derived as

$$\widetilde{u}_B = \frac{u_B}{value} \tag{4}$$

The total relative uncertainty of one measurement was given as

$$\widetilde{u}_{B,tot} = \sqrt{\sum u_B^2} \tag{5}$$

For the surface wave measurements, Equation (2) contains the parameters and assumed deviations Δ given in Table 1.

Table 1. Assumed symmetrical deviations for the parameters in Equation (2), including varying parameters.

Parameter	Value	Deviation	Ref./Origin
Frequency f in Hz	measured	± 10	Pixel resolution
Wavelength λ in m	measured	$\pm 2.00 \times 10^{-6}$	Pixel resolution
Density ρ in kg/m^3	7.874	± 0.063	[52]
Gravity constant g in m/s^2	9.81	$\pm 1.26 \times 10^{-3}$	Committee on Data for Science and Technology (CODATA)

Since the surface waves propagate over a certain surface area, the related temperature was determined as the average of temperatures within the propagation area. Temperature fields were recorded using an RGB-camera (DFK 23GM021, TheImagingSource, Bremen, Germany) at a recording rate of 30 fps, exposure time of 1/200,000 s and a gain of 0 dB. An IR filter was installed to avoid damage to the sensor by the laser light process reflections. The temperature in each pixel of the camera sensor was determined by calculating the intensity ratios between the red and blue pixel intensity values assuming gray body emission (with calibrated offset) and considering the sensor spectral sensitivity curves. Within the measuring area, the minimum and maximum values showed deviations between 2% and 9% from the average values.

2.2. Ion Interaction Calculations

A simplified ion interaction model was implemented in MATLAB (Version 2017a), starting with $10 \times 10 \times 10$ iron (Fe) atoms arranged in a cube at constant initial distances to derive the forces between the Fe atoms, assuming no contamination. A simple Lennard-Jones pair potential was used to describe the atom interactions [11]. It is known that, by using the simple Lennard-Jones potential, metals are typically not completely described, and many body interactions need to be included in the calculations to derive highly accurate results [53]. However, in order to gain knowledge about trends and simple interactions, the simple model can give first indications with little calculation effort. No electron density impacts of neighboring atoms or external fields were used. Comparably large time steps were applied, which leads to reduced accuracy but rapid convergence, since atoms arrange to a comfortable position quite quickly. In combination with the initial atom arrangement based on the thermal expansion at the fixed and constant calculation temperature, the system shows sufficient convergence after only a few calculation steps. The deviation between time steps of the atoms is ~0.1% for all tested temperatures [51]. However, the simplifications using a comparably small number of atoms and a simple pair potential allow

a rapid calculation of the interaction forces between the atoms and the general macroscopic trends can be derived.

Using the mechanical approach to derive surface tension [54], normal and tangential components of the pressure in the ion layers were extracted. The direct neighbor interactions were calculated for all Fe atoms and the resulting forces initiated the atom movements before the next calculation step [51]. It was seen that, already after three iterations, a quasistatic positioning had been arranged [51]. For the surface tension calculations, the results after seven steps were taken. Similar to in [49], the surface tension value of the system was derived, averaging atom forces within the atom layers and a certain thickness. Evaluation lines were defined to determine the tension between the combined ions of the two regions in one layer on each side of the line in both x- and y-direction. The surface tension was determined from averaged force values from the first and second layer (Figure 2).
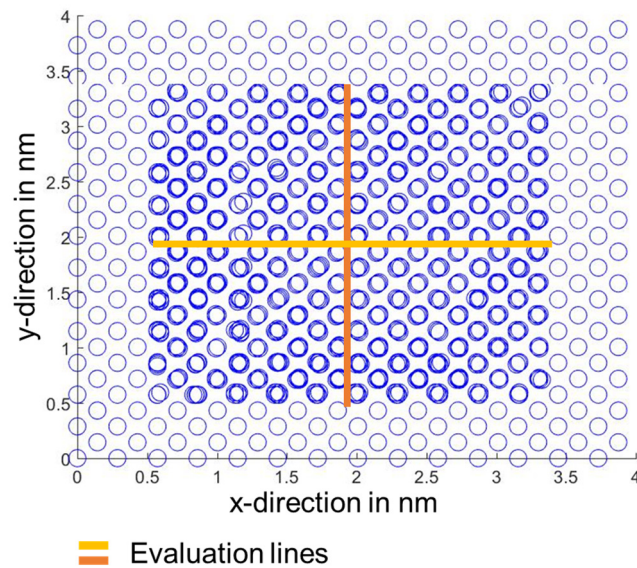

Figure 2. Top view of the calculation system including evaluation lines.

3. Results

3.1. Surface Waves

Surface tension values were derived at high temperatures for steel material using the derivation of surface tension values from the analysis of surface waves. Frequencies and wavelengths of the surface waves were extracted (Figure 3). At increasing temperatures, the waves show a trend towards lower frequencies at increased wavelengths.
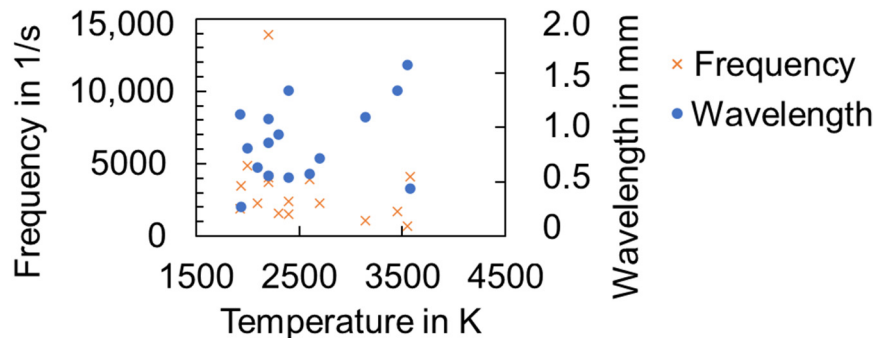

Figure 3. Measurements of surface wave frequencies and wavelengths at multiple temperatures.

3.2. Calculations

The ion interaction calculations were used to calculate the forces within the layers. Evaluation was performed along the evaluation lines separately for each layer and in x-and y-directions (Figure 4). The average forces vary at different temperatures.
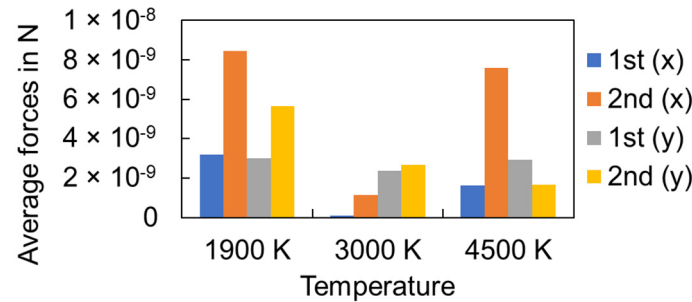

Figure 4. Average forces along the evaluation lines in x- and y-directions in the 1st and 2nd layers.

3.3. Surface Tension

Below the boiling temperature, both the experimental and calculation results show decreasing trends. Below boiling temperature, surface tension values decrease more steeply than the extrapolation of linear assumptions from the literature would imply. Above boiling temperature, surface tension values increase (Figure 5).
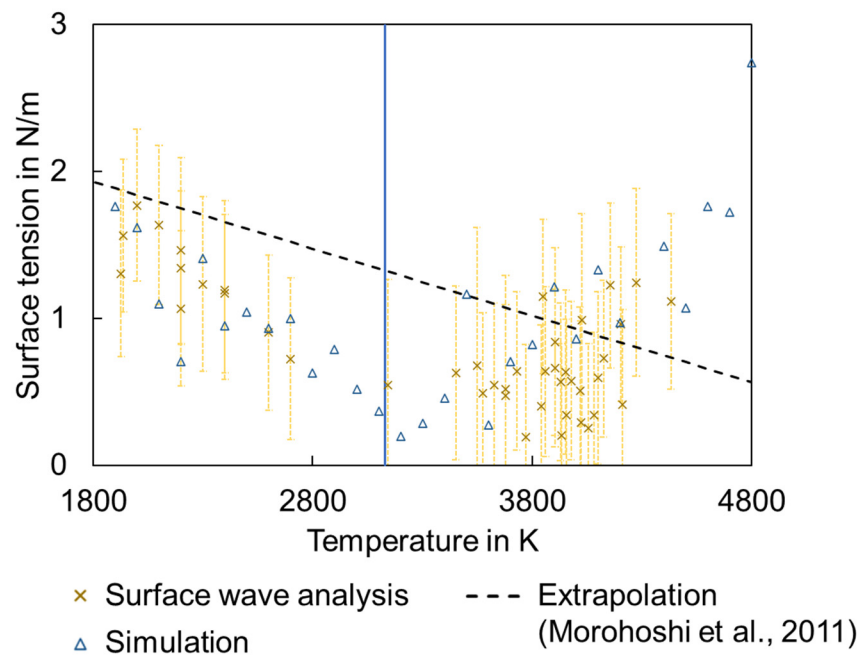

Figure 5. Surface tension measurements and calculations around the boiling temperature of steel, including surface wave analysis, simulation results and extrapolation from Equation (1) [24].

4. Discussion

Both experimental and simulation results show similar global trends. Although simplifications were introduced for the modeling, the global, macroscopic trends in measured surface tension values seem to be possible to reproduce. The presented calculation results are able to show the trends in temperature dependence on surface tension, which was seen also in [45].

The measured and calculated surface tension values in this work deviate from the typically assumed linear decreasing extrapolations in the literature (e.g., Equation (1)) (Figure 5). Below boiling temperature, a tendency, typical for most pure materials, was

seen, showing a decrease in surface tension values with increasing temperature (e.g., [22]). This tendency was also seen in the simulation and surface wave analyses (Figure 5). An exponential decrease was suggested from previous experiments when analyzing surface tension data below boiling temperature [51]. The negative surface tension gradient is typically explained by the reduced bonding forces between the metal ions at elevated temperatures and the increasing distance between them [31]. However, the negative slope of the decrease is larger than expected. Such a steeper decrease was also seen during recent measurements using electromagnetic levitation of pure iron drops [24] and stainless steel drops with acoustic levitation [25]. Niobium also showed a much steeper trend in recent studies compared to earlier literature values [55]. However, the temperature range was around the melting temperature, which leads to the conclusion of a linear trend. The decrease can be assumed to derive from the significantly increased reduction in bonding strength between the ions and the interaction of at least two surface atomic layers, as calculated in the ion interaction model.

Above boiling temperature, the experiments show a tendency to an increase in surface tension values at high temperatures, although uncertainties are still high. The same trend was seen when evaluating model calculations (Figure 5). The suggested method in this work enabled escaping from some restrictions and limitations of typically used surface tension measurement methods and a first insight into surface tension above boiling temperature. However, up to now, no related literature data have been found to compare with the data. Possible explanations for the increasing trend in surface tension values above boiling temperature can be suspected as: (1) the altered surface topology induced by atom losses due to vaporization of the surface layers and (2) the strength and kind of bonding forces between the surface ions. Since the calculation results show the experimentally observed trend and do not consider alterations in the vaporization effects, it can be assumed that the underlying effect is implemented in the current model, which is based on the calculation of forces between the ions in the bulk and surface.

Attractive and repulsive forces act between the ions in the liquid bulk. It is known that, at melting temperature, few bonds are broken, and lattice ions can rearrange [56] until they find an energetically comfortable position. This means that this reordering is mainly driven by repulsive forces between the ions [56]. At increasing temperature, the distances between the ions increase (thermal expansion) and the attracting forces are reduced [27], which enables an even easier ion separation and, in turn, reduced forces in the material surface plane, which should result in reduced surface tension. Increasing the temperature to boiling leads to smaller attraction at higher ion separation according to the pair potential theory (Figure 6).
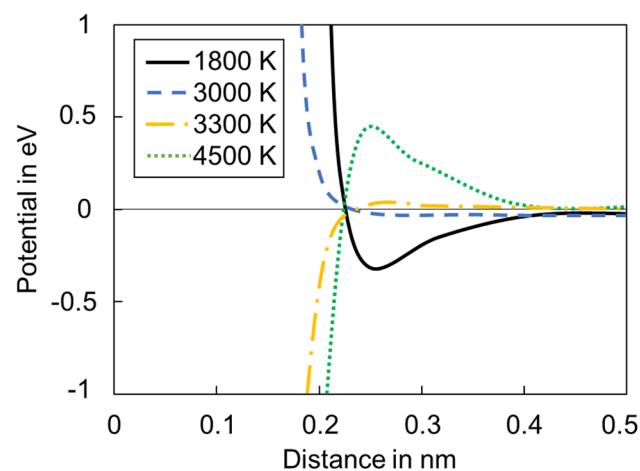

Figure 6. Pair potentials used in the ion calculation below and above boiling temperature.

However, when calculating the pair potential above boiling temperature (Figure 6), ions show similar energetically comfortable distances, but at different slopes of the potential, which should lead to the tendency that ions attract and can easily collapse into each other. Apparently, the collapsing of ions into each other does not occur. High vibrational energies are suspected to have a limited effect on thermal expansion (e.g., [24]), but might be hindering this collapse.

It is known that, above boiling temperature, attractive forces dominate bonding behavior [19]. Latent heats of vaporization and, according to Touton's rule, boiling temperatures are mainly determined by attractive forces between the ions [19]. In other systems, e.g., that of Au, it was found that, at elevated temperatures, the lateral atomic density can increase relatively to the bulk [57], which indicates that an even closer ion packing is possible above boiling, compared to below boiling, temperatures. The altered bonding conditions are in the order of magnitude of the surface tension, which must be of the order of the bind energy divided by the cross-sectional area of the ions [8]. This, in turn, means that the dominating attractive forces in the surface layer can increase at increasing temperature, which can be an explanation for the observed tendencies of increasing surface tension at increasing temperatures in the experiments. This study was focused on steel material. However, the surface tension around boiling temperatures of other metals should show similar trends, even though some other aspects of ion interactions must be considered.

5. Conclusions

Based on surface wave measurements and ion interaction calculations, it can be concluded that the dominating attractive forces above boiling temperature should increase with increasing temperature and lead to increasing surface tension forces in the surface layers of liquid metal.

Data Availability Statement: The raw data supporting the conclusions of this article will be made available by the authors on request.

Conflicts of Interest: The author declares no conflicts of interest.

References

1. Gatzen, M.; Radel, T.; Thomy, C.; Vollertsen, F. The role of zinc layer during wetting of aluminium on zinc-coated steel in laser brazing and welding. *Phys. Procedia* **2014**, *56*, 730–739. [CrossRef]
2. Frostevarg, J.; Kaplan, A.F. Undercuts in laser arc hybrid welding. *Phys. Procedia* **2014**, *56*, 663–672. [CrossRef]
3. Powell, J.; Ilar, T.; Frostevarg, J.; Torkamany, M.J.; Na, S.-J.; Petring, D.; Zhang, L.; Kaplan, A.F.H. Weld root instabilities in fiber laser welding. *J. Laser Appl.* **2015**, *27*, S29008. [CrossRef]
4. Suder, W.; Ganguly, S.; Williams, S.; Yudodibroto, B. Root stability in hybrid laser welding. *J. Laser Appl.* **2017**, *29*, 022410. [CrossRef]
5. Volpp, J.; Vollertsen, F. Keyhole stability during laser welding—Part I: Modeling and evaluation. *Prod. Eng.* **2016**, *10*, 443–457. [CrossRef]
6. Siva Prasad, H.; Brueckner, F.; Volpp, J.; Kaplan, A.F. Laser metal deposition of copper on diverse metals using green laser sources. *Int. J. Adv. Manuf. Technol.* **2020**, *107*, 1559–1568. [CrossRef]
7. Panwisawas, C.; Sovani, Y.; Turner, R.P.; Brooks, J.W.; Basoalto, H.C.; Choquet, I. Modelling of thermal fluid dynamics for fusion welding. *J. Mater. Process. Technol.* **2018**, *252*, 176–182. [CrossRef]
8. Marchand, A.; Weijs, J.H.; Snoeijer, J.H.; Andreotti, B. Why is surface tension a force parallel to the interface? *Am. J. Phys.* **2011**, *79*, 999–1008. [CrossRef]
9. Skapski, A.S. The surface tension of liquid metals. *J. Chem. Phys.* **1948**, *16*, 389–393. [CrossRef]
10. Adam, N.K. *Physics and Chemistry of Surfaces*, 3rd ed.; Interscience Publishers: New York, NY, USA, 1941.
11. Lennard-Jones, J.E.; Dent, B.M. The change in lattice spacing at a crystal boundary. *Proc. R. Soc. Lond. Ser. A Contain. Pap. A Math. Phys. Character* **1928**, *121*, 247–259.
12. Penfold, J. The structure of the surface of pure liquids. *Rep. Prog. Phys.* **2001**, *64*, 777. [CrossRef]
13. DiMasi, E.; Tostmann, H.; Ocko, B.M.; Pershan, P.S.; Deutsch, M. X-ray reflectivity study of temperature-dependent surface layering in liquid Hg. *Phys. Rev. B* **1998**, *58*, R13419. [CrossRef]

14. Regan, M.J.; Kawamoto, E.H.; Lee, S.; Pershan, P.S.; Maskil, N.; Deutsch, M.; Magnussen, O.M.; Ocko, B.M.; Berman, L.E. Surface layering in liquid gallium: An X-ray reflectivity study. *Phys. Rev. Lett.* **1995**, *75*, 2498. [CrossRef] [PubMed]

15. Zhao, M.; Chekmarev, D.S.; Cai, Z.H.; Rice, S.A. Structure of liquid Ga and the liquid-vapor interface of Ga. *Phys. Rev. E* **1997**, *56*, 7033. [CrossRef]

16. Velasco, E.; Tarazona, P.; Reinaldo-Falagán, M.; Chacón, E. Low melting temperature and liquid surface layering for pair potential models. *J. Chem. Phys.* **2002**, *117*, 10777–10788. [CrossRef]

17. Gogate, D.V.; Kothari, D.S.X.C. On the theory of surface tension of liquid metals. *Lond. Edinb. Dublin Philos. Mag. J. Sci.* **1935**, *20*, 1136–1144. [CrossRef]

18. Sides, S.W.; Grest, G.S.; Lacasse, M.D. Capillary waves at liquid-vapor interfaces: A molecular dynamics simulation. *Phys. Rev. E* **1999**, *60*, 6708. [CrossRef]

19. Israelachvili, J.N. *Intermolecular and Surface Forces*; Elsevier Science: Amsterdam, The Netherlands, 2010.

20. Baskes, M.I. Modified embedded-atom potentials for cubic materials and impurities. *Phys. Rev. B* **1992**, *46*, 2727. [CrossRef] [PubMed]

21. Evans, R. A pseudo-atom theory for the surface tension of liquid metals. *J. Phys. C: Solid State Phys.* **1974**, *7*, 2808. [CrossRef]

22. Keene, B.J. Review of data for the surface tension of pure metals. *Int. Mater. Rev.* **1993**, *38*, 157–192. [CrossRef]

23. Wille, G.; Millot, F.; Rifflet, J.C. Thermophysical properties of containerless liquid iron up to 2500 K. *Int. J. Thermophys.* **2002**, *23*, 1197–1206. [CrossRef]

24. Morohoshi, K.; Uchikoshi, M.; Isshiki, M.; Fukuyama, H. Surface tension of liquid iron as functions of oxygen activity and temperature. *ISIJ Int.* **2011**, *51*, 1580–1586. [CrossRef]

25. Klapczynski, V.; Le Maux, D.; Courtois, M.; Bertrand, E.; Paillard, P. Surface tension measurements of liquid pure iron and 304L stainless steel under different gas mixtures. *J. Mol. Liq.* **2022**, *350*, 118558. [CrossRef]

26. Finke, B.R.; Simon, G. On the gas kinetics of laser-induced evaporation of metals. *J. Phys. D Appl. Phys.* **1990**, *23*, 67. [CrossRef]

27. Padmavathi, D.A. Potential energy curves & material properties. *Mater. Sci. Appl.* **2011**, *2*, 97–104.

28. Tang, K.; Kawka, P.; Buckius, R. Geometric optics applied to rough surfaces coated with an absorbing thin film. *J. Thermophys. Heat Transf.* **1999**, *13*, 169–176. [CrossRef]

29. Schott, P.; de Beaucoudrey, N.; Bourlier, C. Reflectivity of one-dimensional rough surfaces using the ray tracing technique with multiple reflections. In Proceedings of the International Geoscience and Remote Sensing Symposium, Toulouse, France, 21–25 July 2003; Volume 7, pp. 4214–4216.

30. Tostmann, H.; DiMasi, E.; Pershan, P.S.; Ocko, B.M.; Shpyrko, O.G.; Deutsch, M. Surface structure of liquid metals and the effect of capillary waves: X-ray studies on liquid indium. *Phys. Rev. B* **1999**, *59*, 783. [CrossRef]

31. Knight, C.J. Theoretical modeling of rapid surface vaporization with back pressure. *AIAA J.* **1979**, *17*, 519–523. [CrossRef]

32. Drelich, J.; Fang, C.; White, C.L. Measurement of interfacial tension in fluid-fluid systems. *Encycl. Surf. Colloid Sci.* **2002**, *3*, 3158–3163.

33. Schuster, J.M.; Schvezov, C.E.; Rosenberger, M.R. Influence of experimental variables on the measure of contact angle in metals using the sessile drop method. *Procedia Mater. Sci.* **2015**, *8*, 742–751. [CrossRef]

34. Trinh, E.H.; Marston, P.L.; Robey, J.L. Acoustic measurement of the surface tension of levitated drops. *J. Colloid Interface Sci.* **1988**, *124*, 95–103. [CrossRef]

35. Egry, I.; Lohoefer, G.; Jacobs, G. Surface tension of liquid metals: Results from measurements on ground and in space. *Phys. Rev. Lett.* **1995**, *75*, 4043. [CrossRef] [PubMed]

36. Fahimi, K.; Mädler, L.; Ellendt, N. Measurement of surface tension with free-falling oscillating molten metal droplets: A numerical and experimental investigation. *Exp. Fluids* **2023**, *64*, 133. [CrossRef]

37. Ozawa, S.; Suzuki, S.; Hibiya, T.; Fukuyama, H. Influence of oxygen partial pressure on surface tension and its temperature coefficient of molten iron. *J. Appl. Phys.* **2011**, *109*, 014902. [CrossRef]

38. Leitner, T.; Klemmer, O.; Pottlacher, G. Bestimmung der temperaturabhängigen Oberflächenspannung des Eisen-Nickel-Systems mittels elektromagnetischer Levitation. *tm-Tech. Mess.* **2017**, *84*, 787–796. [CrossRef]

39. Kolevzon, V. Temperature dependence of surface tension and capillary waves at liquid metal surfaces. *J. Exp. Theor. Phys.* **1998**, *87*, 1105–1109. [CrossRef]

40. Shmyrov, A.; Mizev, A.; Shmyrova, A.; Mizeva, I. Capillary wave method: An alternative approach to wave excitation and to wave profile reconstruction. *Phys. Fluids* **2019**, *31*, 012101. [CrossRef]

41. Nikolić, D.; Nešić, L. Determination of surface tension coefficient of liquids by diffraction of light on capillary waves. *Eur. J. Phys.* **2012**, *33*, 1677. [CrossRef]

42. Minami, Y. Surface tension measurement of liquid metal with inelastic light-scattering spectroscopy of a thermally excited capillary wave. *Appl. Phys. B* **2014**, *117*, 969–972. [CrossRef]

43. Bennett, T.D.; Grigoropoulos, C.P.; Krajnovich, D.J. Near-threshold laser sputtering of gold. *J. Appl. Phys.* **1995**, *77*, 849–864. [CrossRef]

44. Shen, L.; Denner, F.; Morgan, N.; van Wachem, B.; Dini, D. Capillary waves with surface viscosity. *J. Fluid Mech.* **2018**, *847*, 644–663. [CrossRef]

45. Chen, M.; Yang, C.; Guo, Z.Y. A Monte Carlo simulation on surface tension of liquid nickel. *Mater. Sci. Eng. A* **2000**, *292*, 203–206. [CrossRef]

46.   Heinz, H.; Vaia, R.A.; Farmer, B.L.; Naik, R.R. Accurate simulation of surfaces and interfaces of face-centered cubic metals using 12− 6 and 9− 6 Lennard-Jones potentials. *J. Phys. Chem. C* **2008**, *112*, 17281–17290. [CrossRef]

47.   Belashchenko, D.K.; Kravchunovskaya, N.E.; Ostrovski, O. Molecular dynamics calculation of surface tension of liquid metals using the embedded atom model. *Calphad* **2010**, *34*, 45–50. [CrossRef]

48.   Chen, M.; Yang, C.; Guo, Z.Y. Surface tension of Ni-Cu alloys: A molecular simulation approach. *Int. J. Thermophys.* **2001**, *22*, 1295–1302. [CrossRef]

49.   Yousefi, E.; Sun, Y.; Kunwar, A.; Guo, M.; Moelans, N.; Seveno, D. Surface tension of aluminum-oxygen system: A molecular dynamics study. *Acta Mater.* **2021**, *221*, 117430. [CrossRef]

50.   Hou, H.Y.; Chen, G.L.; Chen, G.; Shao, Y.L. A molecular dynamics simulation on surface tension of liquid Ni and Cu. *Comput. Mater. Sci.* **2009**, *46*, 516–519. [CrossRef]

51.   Volpp, J. Surface tension of steel at high temperatures. *SN Appl. Sci.* **2023**, *5*, 237. [CrossRef]

52.   Assael, M.J.; Kakosimos, K.; Banish, R.M.; Brillo, J.; Egry, I.; Brooks, R.; Quested, P.N.; Mills, K.C.; Nagashima, A.; Sato, Y.; et al. Reference data for the density and viscosity of liquid aluminum and liquid iron. *J. Phys. Chem. Ref. Data* **2006**, *35*, 285–300. [CrossRef]

53.   Masuda, S.; Sawada, S. Molecular dynamics study of size effect on surface tension of metal droplets. *Eur. Phys. J. D* **2011**, *61*, 637–644. [CrossRef]

54.   Buff, F.P. Spherical interface. II. Molecular theory. *J. Chem. Phys.* **1955**, *23*, 419–427. [CrossRef]

55.   Le Maux, D.; Klapczynski, V.; Courtois, M.; Pierre, T.; Le Masson, P. Surface tension of liquid Fe, Nb and 304L SS and effect of drop mass in aerodynamic levitation. *J. Mater. Sci.* **2022**, *57*, 12094–12106. [CrossRef]

56.   Israelachvili, J.; Min, Y.; Akbulut, M.; Alig, A.; Carver, G.; Greene, W.; Kristiansen, K.; Meyer, E.; Pesika, N.; Rosenberg, K.; et al. Recent advances in the surface forces apparatus (SFA) technique. *Rep. Prog. Phys.* **2010**, *73*, 036601. [CrossRef]

57.   Celestini, F.; Ercolessi, F.; Tosatti, E. Can liquid metal surfaces have hexatic order? *Phys. Rev. Lett.* **1997**, *78*, 3153. [CrossRef]